Fine structure of the H_2 $5g-4f$ inter-Rydberg transition revealed by difference frequency laser spectroscopy

D. Uy,[a] C. M. Gabrys, and T. Oka
Department of Chemistry and Department of Astronomy and Astrophysics, The University of Chicago, Chicago, Illinois 60637

B. J. Cotterell and R. J. Stickland[b]
Department of Chemistry, University of Wales, Cardiff, P.O. Box 912, Cardiff CF10 3TB, United Kingdom

Ch. Jungen and A. Wüest[c]
Laboratoire Aimé Cotton, Centre National de la Recherche Scientifique, Campus D'Orsay, Batiment 505, 91405 Orsay Cedex, France

(Received 7 August 2000; accepted 15 September 2000)

The spectrum of the $5g-4f$ inter-Rydberg band of H_2 has been recorded with a difference frequency laser system and analyzed using multichannel quantum defect theory (MQDT). New transitions have been observed; in addition to the singlet–triplet splittings previously observed, the hyperfine structure of the ortho-hydrogen spectrum is partially resolved in the present experiment. MQDT is used to analyze the data in a two stage process. First, the *ab initio* MQDT predictions were refined by fitting the quantum defect functions over a range of internuclear separation R. Second, $4f$ singlet and triplet quantum defects are extracted from the para-hydrogen spectra, i.e., those lines without complicating hyperfine structure. This information was then used to calculate the fine structure of a sample ortho-hydrogen line, $R_3(2)v^+=0$. While the spectra are predominantly composed of absorption lines, some transitions from high vibrational levels of the $5g$ triplet manifold to $4f$ triplet levels are observed in stimulated emission. © *2000 American Institute of Physics.* [S0021-9606(00)01446-X]

I. INTRODUCTION

The spectroscopic study of high-l Rydberg states in diatomic molecules effectively started with the observation of the $4f$-$X\,^2\Pi$ system of NO by Jungen and Miescher.[1] These authors based their description of the nearly nonpenetrating molecular $4f$ electron and its interaction with the NO^+ core on a paper by Buckingham[2] on long-range intermolecular forces. Since then, studies of high-l Rydberg states have been made on a number of molecular species, including H_2 (see, for example, Basterrechea, Davies, Smith, Stickland,[3] and references therein), NO (see, for example, Martin, Stickland, Martin, Davies,[4] and references therein), and, more recently, N_2 (Huber, Jungen, Yoshino, Ito, and Stark[5]), and the triatomics CO_2 (Dobber, Buma, and de Lange[6]) and H_2O (Child and Glab[7]). Herzberg and Jungen[8] published the first spectral observations and assignments of infrared transitions between high-l states of H_2, for the $5g-4f$ and $4f-3d$ transitions. Since then, various transitions have been observed involving intercombinations of the high-l Rydberg states $3d$, $4d$, $4f$, $5f$, $5g$, $6g$, $6h$, $7h$, $7i$, and $8i$ using Fourier-transform infrared (FTIR) spectroscopy[9,10] and diode laser spectroscopy.[3,11,12] Also, microwave spectroscopy (see, for example, Sturrus, Hessels, Arcuni, Lundeeen,[13] and references therein) has been used to study inter-Rydberg transitions with $n>9$ to very high precision. In the absence of autoionization or predissociation, these high-l states have lifetimes which are long enough to allow very precise determination of their energies.

Two theoretical approaches have been applied to the calculation of high-l molecular Rydberg states: The Hamiltonian diagonalization technique[8,11,14] and multichannel quantum defect theory (MQDT),[9,10,15] both of which are based on the multipole polarization model originally used for the calculation of atomic high-l states. As the Rydberg state quantum numbers n and l increase, the results from these two methods tend to converge (assuming the diagonalization of the large matrices generated by the first method is feasible) since the long-range physics is the same in both techniques, and electron–core interactions become weaker. Conversely, core-penetrating p and d Rydberg states cannot be calculated accurately using the multipole model since the coupling between the molecular core and the Rydberg electron is too strong. For intermediate values of n, l such as the $4f$ state, the *ab initio* energy levels for H_2 have been found[10,11] to be in error by up to 0.5 cm^{-1} for $v^+=0$. Due to the intrinsic error in the first principles calculation of the $4f$ state, a fitting procedure will be introduced in the present work.

The experiment described in this paper began as an accidental observation of a large number of very strong lines with negative-ion derivative line shapes during a search for the CH_5^+ spectrum in positive column discharges. Observation of such spectral lines had been experienced earlier in the

[a]Present address: Physics Department, Ford Research Laboratory, Mail Drop 3028/SRL, P.O. Box 2053, Dearborn, MI 48121.
[b]Electronic mail: stickland@cardiff.ac.uk
[c]Present address: Laboratorium für Physikalische Chemie, ETH Zürich, Zürich CH-8092, Switzerland.

velocity-modulated spectra of hydrogen-dominated plasmas. A more systematic study of the spectrum was highly desirable. Compared with the earlier work of Jungen, Dabrowski, Herzberg, and Vervloet[10] using FTIR spectroscopy and Davies, Guest, and Stickland[12] using diode laser spectroscopy, the difference frequency laser spectrum was obtained with higher sensitivity and resolution, permitting a closer study of the fine structure of the $5g-4f$ Rydberg transition. In addition to the more extensive theoretical analysis, new experimental findings in this work are the presence of hyperfine structure for the ortho-hydrogen species and the observation of a population anomaly in the triplet states leading to stimulated emission in certain higher vibrational levels. A description of the method of H_2 Rydberg state detection in velocity modulation experiments is proposed.

II. EXPERIMENT

The spectrum was recorded with a difference frequency system previously described by Bawendi, Rehfuss, and Oka.[16] Radiation from an argon ion laser and a tunable ring dye laser were combined collinearly in a nonlinear crystal, $LiNbO_3$. By properly temperature-tuning the crystal for phase matching, radiation with a frequency equal to the difference of the frequencies of the dye and argon ion lasers is generated. Ten per cent of the resulting infrared radiation is used for reference frequency calibration, while the rest of the beam is sent to the discharge cell. This cell is a one-meter long, liquid nitrogen cooled glass tube with 18 pairs of inlets and multiple outlets, designed to maximize fresh plasma chemical reactions through the cell. The infrared (IR) laser beam was propagated through the discharge tube in a multicyclic path arrangement. It was first divided into two with a ZnSe beamsplitter, and then passed through the cell four times each in opposite directions. Since the initial objective was to look for CH_5^+, a gas mixture of 30–60 mT of methane, and around 600 mT of hydrogen was used. Test experiments using pure H_2 showed that the presence of the small amount of methane does not affect the H_2 Rydberg spectra. The plasma was produced in a 6 kHz ac (alternating current) glow discharge used for velocity modulation experiments, and the signals detected by two InSb detectors and processed by a lock-in amplifier. Spectra were measured from 2536 to 2424 cm^{-1} using N_2O absorption lines for calibration.[17] More than 500 spectral lines were observed in this region, of which around one-third has been assigned to the $5g-4f$ Rydberg spectrum. A complete list of these lines is available from the EPAPS archive.[31] Aside from the hydrogen Rydberg signals, a number of H_3^+ transitions were observed, as well as the Brackett (α) transition of the hydrogen atom. The unassigned lines probably include weak high vibrational transitions of the $5g-4f$ band, and the $5f-4d$ inter-Rydberg spectrum of H_2. The strongest H_2 Rydberg transition had a signal-to-noise ratio of around 450.

A. H_2 Rydberg state production and detection

The observation of the strong H_2 Rydberg spectral lines using velocity modulation is surprising because this technique is supposed to apply only to charged species. Nevertheless, these spectral lines are often observed in studies using hydrogen dominated plasmas. The observed derivative shape which is opposite to that for cations (see Fig. 1) clearly indicates that the Rydberg H_2 molecules are accelerated towards the anode like negative ions. We interpret this acceleration as due to the momentum transfer from plasma electrons to H_2 during the process of electron impact excitation of the ground-state H_2 molecules to the excited Rydberg states. Since the electrons have average energies of a few to several electron volts in our discharge, the electron impact excitation must be effected by high-energy electrons at the tail of the Boltzmann energy distribution. The excitation starts from the threshold electron energy of ~14 eV and is maximum for ~30 eV.[18] Such electrons have velocities two orders of magnitude less than that of light. A simple classical momentum transfer calculation shows that, if such electrons collide with neutral H_2, the latter are accelerated to the velocity of ~1000 $m\,s^{-1}$. The H_2 molecules in the Rydberg state with the highest angular momenta, such as the $5g$ and $4f$ states, cascade down by spontaneous emission and collisions with H_2. The spontaneous emission time for the $4f-3d$ transition is about 7×10^{-8} seconds estimated from the Einstein coefficient for the transition in the hydrogen atom.[19] At the pressure of 0.6 Torr used in the experiment, the excited H_2 molecules may undergo a few collisions with the ground-state H_2 in the plasma. The collisions may quench the electronic excitation, elastically slow down the molecule, or the electronic excitation may hop from the excited-state H_2 to the ground-state H_2. The excitation and the translational energy of the Rydberg hydrogen will be lost quickly after several collisions but, on the average, the observed Rydberg H_2 retains its acceleration. An average velocity of 300–500 $m\,s^{-1}$ would be sufficient to modulate the signal efficiently.

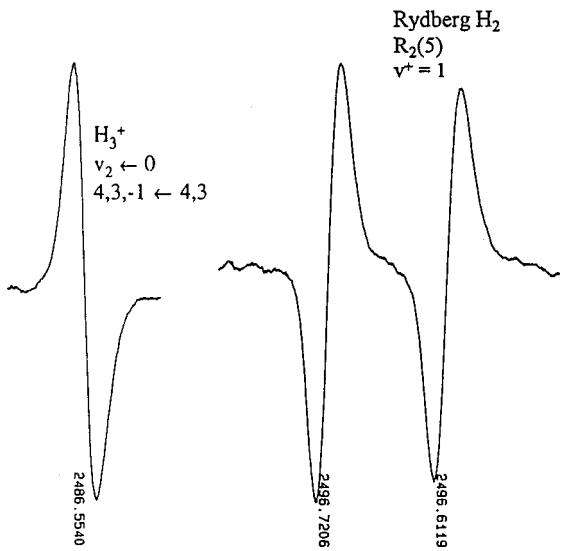

FIG. 1. Difference frequency laser spectra of the H_3^+ v_2 4,3,−1←4,3 rovibrational transition and the H_2 $5g-4f$ $R_2(5)v^+=1$ Rydberg transition illustrating opposite phase observed by velocity modulation in a plasma discharge.

Compared with the vibrational transitions of H_3^+ whose transition dipole moment is 0.156 Debye, the $5g-4f$ Rydberg transition of H_2 has a huge dipole moment of 45

Debye.[19] The large H_2/H_3^+ intensity ratio of $\sim 8\times 10^4$ plus partitioning into fewer vibration–rotation states make the H_2 Rydberg signal potentially much stronger than that of H_3^+. From the observed approximate equal intensities between the two spectra, and the well-known approximate concentration of $3\times 10^{10}\,\mathrm{cm}^{-3}$ of H_3^+ in hydrogen dominated plasmas, we estimate the concentration of Rydberg H_2 in the $4f$ state to be $\sim 1\times 10^5\,\mathrm{cm}^{-3}$. The spontaneous emission rate from the $4f$ state[19] is $\sim 1.4\times 10^7\,\mathrm{s}^{-1}$. The collisional quenching rate of H_2 Rydberg states has not been measured. Dehmer and Chupka[20] assumed this rate to be equal to the rate of the ion–neutral reaction $H_2^+ + H_2 \rightarrow H_3^+ + H$ and determined it based on the measurement of Shao and Ng.[21] If we adopt the Dehmer–Chupka model, the quenching rate at our pressure ($\sim$0.6 Torr) is $4.9\times 10^7\,\mathrm{s}^{-1}$. Thus the total loss rate of the $4f$ Rydberg state is $\sim 6.3\times 10^7\,\mathrm{s}^{-1}$. In order to maintain the number density of $1\times 10^5\,\mathrm{cm}^{-3}$, a production rate of H_2 in the $4f$ state of $6\times 10^{12}\,\mathrm{cm}^{-3}\,\mathrm{s}^{-1}$ is needed.

The order of magnitude of this production rate can be explained by the electron velocity of $10^8\,\mathrm{cm\,s}^{-1}$, estimated electron density of $\sim 3\times 10^{10}\,\mathrm{cm}^{-3}$, the excitation cross-section of $\sim 10^{-21}\,\mathrm{cm}^2$ and the H_2 density in our plasma of $1.7\times 10^{16}\,\mathrm{cm}^{-3}$.

It has been observed that, when helium is added to hydrogen in the plasma, the intensities of the H_2 Rydberg spectral lines decrease, while those of H_3^+ increase. With the helium pressure higher than the hydrogen pressure, the Rydberg lines disappear completely. The decrease of the Rydberg hydrogen versus the increase of H_3^+ by helium is explained by the dominance of the Penning ionization

$$H_2 + He^* \rightarrow H_2^+ + He + e^-, \tag{1}$$

over the Penning excitation[22]

$$H_2 + He^* \rightarrow H_2^* + He, \tag{2}$$

when the threshold for ionization is met, and by the subsequent extremely efficient ion–neutral reaction

$$H_2^+ + H_2 \rightarrow H_3^+ + H. \tag{3}$$

III. OBSERVED SPECTRA AND ANALYSIS

The spectrum was initially assigned using *ab initio* predictions. The published FTIR data[10] proved useful in the analysis, since the FTIR relative intensity measurements across the whole band are more accurate than those yielded by the present experiment: The difference frequency spectrum is recorded in many sections, and these are not normalized against one another. Intensity measurements and calculations are very important in the analysis of spatially diffuse high-l Rydberg systems, since an enormous number of transitions are possible, but relatively few of these have appreciable intensity even at the temperatures observed in plasma discharges. Also, both absorption and emission processes were observed in the spectra. One consequence of this is that the singlet and triplet lines cannot be assigned on the basis of the observed relative intensities. This is discussed more fully in Sec. V.

The difference frequency laser system provides greater sensitivity and resolution than the FTIR experiment, and greater coverage was obtained in this study than that obtained in the diode laser investigations;[12] consequently, a large number of lines not seen in previous studies were observed. These included many weak Q branch lines and a few even weaker P branch lines whereas in the original studies only R-branch lines had been observed. These Q and P branch observations can be used to confirm the R branch assignments: the difference between two transitions from the same $4f$ level gives a $5g$ combination difference, for which the *ab initio* model will (for the reasons outlined below) generally give a better prediction than that obtained for the $5g-4f$ transition frequency.

The present experiment easily resolves the singlet and triplet splitting observed previously;[10,12] for example, the singlet and triplet lines of $R_2(5)v^+=1$ are shown in Fig. 1. Such splitting decreases rapidly with l. Singlet–triplet splitting was not observed in the diode laser work[12] on the $6h-5g$ system of H_2, and since this work obtained similar resolution to that of the present experiment it is obvious that the observed splitting is essentially due to the $4f$ state. The presently available *ab initio* calculations, however, do not include the electron exchange effects necessary to calculate such a splitting.

The line assignments are shown in Table I along with the (observed–calculated) differences corresponding to the *ab initio* predictions which were used for the analysis. These differences correspond to the mean frequency of the singlet and triplet lines wherever a pair of lines was observed.

IV. THEORY

A. General description

The multichannel quantum defect theory model of Jungen which has previously been used to account for FTIR spectra of the $5g-4f$ system[10] and $6g-5f$ and $6h-5g$ systems[9] of H_2 and D_2 was used for the calculations and was extended to account for electron and nuclear spins.

The high-l states involved in these transitions show behavior which approximates to Hund's case d coupling. The system can be considered to be composed of two parts: A core H_2^+ ion and a hydrogenic Rydberg electron. The main quantum numbers used to describe these states are the core vibration v^+, the core rotation N^+, the orbital angular momentum l, the principal quantum number n, and the total angular momentum excluding spin N, which is formed by the vector coupling of N^+ and l. In addition the electron and nuclear spins must be included in order to explain the fine details observed in the present results.

The *ab initio* multichannel quantum defect theory has already been described.[9] The present extension preserves the main stages of the calculation, viz: First, the interaction of the Rydberg electron with the fixed core is evaluated for a selected set of values of the internuclear separation R. Sec-

TABLE I. Assigned transitions in the $5g-4f$ system of H_2 against results of MQDT fits. $S=$''singlet,'' $T=$''triplet'' (all in cm^{-1} units).

Transition	Observed		Obs−calc (*ab initio*)	Obs−calc (fit)	Transition	Observed		Obs-calc (*ab initio*)	Obs-calc (fit)
	S	*T*				*S*	*T*		
$Q_1(3)v^+=2$	2444.903	2444.953	0.024	−0.037	$R_0(3)v^+=0$	2484.829	2484.901	−0.226	−0.021
$Q_1(3)v^+=1$	2446.333	2446.382	−0.008	0.074	$Q_3(2)v^+=0$	2486.232	2486.287	−0.069	−0.002
$Q_1(3)v^+=0$	2448.155	2448.200	−0.032	−0.075	$R_2(2)v^+=0$	2487.133	2487.198	−0.013	−0.029
$Q_2(3)v^+=2$	2456.126	2456.177	−0.459	−0.025	$R_1(4)v^+=0$	2489.306	2489.362	−0.231	−0.006
$Q_2(3)v^+=1$		2457.907	−0.378	−0.013	$R_0(3)v^+=1$	2489.604	2489.675	−0.291	0.064
$Q_2(3)v^+=0$	2459.316	2459.367	−0.272	−0.035	$Q_3(2)v^+=1$	2489.973	2490.028	−0.087	−0.076
$R_1(3)v^+=1$	2459.444	2459.492	−0.026	0.054	$R_3(2)v^+=0$	2490.243	2490.297	−0.075	−0.005
$R_1(3)v^+=0$	2459.538	2459.582	−0.051	0.007	$R_2(2)v^+=1$	2491.009	2491.072	0.054	0.019
$R_1(3)v^+=2$	2459.949	2460.005	0.041	−0.014	$R_2(5)v^+=0$	2491.545	2491.617	−0.249	−0.005
$Q_3(4)v^+=1$	2460.361[a]		⋯	⋯	$R_3(6)v^+=0$	2493.359[b]	2493.448[b]	(0.091)	(0.353)
$R_1(3)v^+=3$	2461.415	2461.463	0.232	0.013	$R_1(4)v^+=1$	2494.223	2494.284	−0.367	0.074
$Q_3(4)v^+=0$	2461.596	2461.675	−0.203	0.030	$R_3(2)v^+=1$	2494.594	2494.649	−0.115	−0.103
$R_3(4)v^+=1$	2462.507[a]		⋯	⋯	$R_5(8)v^+=0$	2495.133	2495.189	−0.282	0.025
$R_2(3)v^+=2$	2462.858	2462.907	−0.386	0.049	$R_0(3)v^+=2$	2495.733	2495.843	−0.320	−0.071
$R_3(4)v^+=0$	2463.456	2463.531	−0.218	0.015	$R_2(5)v^+=1$	2496.612	2496.721	−0.329	0.064
$R_2(3)v^+=1$	2463.629	2463.685	−0.376	−0.012	$R_3(6)v^+=1$	2498.287	2498.356	−0.313	0.089
$R_2(3)v^+=0$	2464.281	2464.330	−0.252	−0.014	$Q_1(4)v^+=0$	2498.428	2498.483	−0.245	−0.021
$Q_2(4)v^+=0$	2464.874	2464.936	−0.004	0.039	$R_1(2)v^+=0$	2498.630	2498.678	−0.304	−0.036
$R_2(4)v^+=0$	2464.874	2464.936	−0.031	0.013	$Q_2(5)v^+=0$		2499.457[a]	⋯	⋯
$R_2(4)v^+=1$	2465.489	2465.559	0.015	0.068	$R_1(4)v^+=2$	2500.357	2500.418	−0.331	−0.067
$Q_2(4)v^+=1$		2465.642[a]	⋯	⋯	$R_5(8)v^+=1$	2500.698[a]		⋯	⋯
$P_3(3)v^+=0$	2466.099	2466.146	−0.168	−0.047	$Q_3(1)v^+=0$	2501.057	2501.096	−0.271	0.020
$R_2(4)v^+=2$	2466.553[a]		⋯	⋯	$Q_5(8)v^+=0$	2501.686	2501.742	−0.306	0.002
$Q_2(4)v^+=2$	2466.711[a]		⋯	⋯	$R_2(5)v^+=2$	2502.895	2502.991	−0.341	−0.062
$R_5(5)v^+=0$	2468.338	2468.384	−0.250	−0.053	$R_0(3)v^+=3$	2503.878[a]		⋯	⋯
$R_3(5)v^+=1$	2468.752	2468.803	0.048	0.088	$R_3(6)v^+=2$	2504.315[b]	2504.354[b]	(−0.735)	(−0.443)
$Q_3(5)v^+=0$	2469.461	2469.508	0.015	0.056	$R_3(1)v^+=0$	2504.354	2504.401	−0.249	0.041
$R_4(6)v^+=0$	2469.610	2469.663	−0.002	0.042	$R_1(2)v^+=1$	2504.753	2504.787	−0.396	0.054
$Q_3(3)v^+=0$	2470.112	2470.156	−0.173	−0.052	$Q_2(5)v^+=1$	2505.645	2505.763	−0.357	0.034
$R_3(5)v^+=2$	2470.345	2470.400	0.155	−0.012	$R_4(7)v^+=2$	2506.176	2506.214	−0.314	−0.015
$Q_3(5)v^+=1$	2470.734	2470.787	0.079	0.119	$R_2(1)v^+=0$	2506.330	2506.397	−0.457	−0.023
$Q_3(3)v^+=1$	2471.152	2471.195	−0.423	−0.210	$Q_3(6)v^+=1$	2506.559	2506.617	−0.348	0.053
$Q_3(3)v^+=2$	2471.414	2471.444	−0.256	−0.114	$Q_3(1)v^+=1$	2507.486[a]		⋯	⋯
$R_3(3)v^+=0$	2473.781	2473.823	−0.164	−0.042	$R_1(4)v^+=3$	2508.286	2508.387	−0.130	0.038
$R_5(7)v^+=2$	2474.655[a]		⋯	⋯	$R_2(5)v^+=3$	2510.891	2510.989	−0.153	0.027
$R_3(3)v^+=1$	2475.399	2475.441	−0.393	−0.183	$R_3(1)v^+=1$	2511.225[a]		⋯	⋯
$R_3(3)v^+=2$	2476.306	2476.345	−0.202	−0.060	$R_3(0)v^+=0$	2511.340	2511.400	−0.623	0.029
$P_4(3)v^+=0$	2477.096	2477.161	−0.109	−0.032	$R_1(2)v^+=2$	2512.093	2512.181	−0.420	−0.077
$Q_5(4)v^+=0$	2477.486	2477.536	−0.136	−0.042	$Q_1(4)v^+=2$	2512.458	2512.519	−0.310	−0.046
$R_3(3)v^+=3$	2477.931	2477.961	−0.066	0.038	$R_3(6)v^+=3$	2512.842	2512.928	−0.117	0.073
$R_5(4)v^+=0$	2480.299	2480.358	−0.132	−0.038	$R_2(1)v^+=1$	2513.712	2513.760	−0.621	0.079
$Q_4(3)v^+=0$	2480.299	2480.358	−0.116	−0.039	$R_3(0)v^+=1$	2519.733	2519.796	−0.843	−0.006
$Q_2(2)v^+=0$	2480.934	2480.995	0.008	−0.009	$R_1(2)v^+=3$	2521.271	2521.343	−0.250	0.010
$R_4(3)v^+=0$	2483.575	2483.639	−0.101	−0.024	$R_2(1)v^+=2$	2522.427	2522.456	−0.746	−0.034
$Q_2(2)v^+=1$	2483.882	2483.945	0.109	0.074					

[a]lines excluded from the fit as only one line was observed.
[b]*R* branch lines omitted from the fit because of their large residuals.

ond, bound Rydberg levels are evaluated for each l and Λ value over appropriate ranges of n and all selected R values. These are subsequently converted into body frame quantum defect functions depending on the electron energy ε as well as R. Finally, the quantum defect functions generated in the second stage are introduced into the rovibrational multichannel quantum defect calculation in the way described by Ross and Jungen.[23] This calculation then yields the rovibronic energies.

The case (d) quantum numbers v^+ and N^+ are not strictly good, since weak rovibronic interactions occur between levels having the same total angular momentum and parity but different values of v^+ and/or N^+. For example, it is known[9] that there is a perturbation involving the states $4f$, $v^+=1$, $N^+=3$ and $5f$, $v^+=0$, $N^+=1$. This interaction is accounted for in the present theoretical approach. However, it is found that v^+ and N^+ are approximately good in most cases, and thus it is reasonable to assign the levels using them.

The transitions observed in studies such as this obey the ''frozen core'' approximation. This means that appreciable transition intensities occur only for transitions which leave the core quantum numbers v^+ and N^+ unchanged. N, however, does change. The transitions are labeled P, Q, and R to indicate $\Delta N=-1$, 0, and $+1$, respectively. Transitions for which $\Delta l=\Delta N$ are strongest; thus the R branch transitions are the most intense in this study. The assignment conven-

tion used in this paper is $\Delta N_N+(N'')v^+$, where ΔN is P, Q, or R as defined above.

B. Determination of body-frame quantum defects

The FTIR study[10] of the $5g-4f$ system of H_2 revealed that the agreement between the *ab initio* predictions and the experimental observations was poor in comparison with that obtained for the $n=6-5$ systems studied:[9] The assigned lines typically show errors of up to 0.5 cm^{-1} (more in a few cases), as can be seen from Table I. This is to be expected since the medium range force contributions to the $4f$ energies are large in comparison with those of the higher n, l states. The vast majority of the error in the calculation of the transition frequency can be ascribed to the $4f$ state for this reason. This expectation is confirmed by the fact that the $6h-5g$ system is reproduced quite well by the theory.[9] Further confirmation comes from the newly observed Q and P transitions. Compare for example the $Q_2(3)v^+=0$ and $R_2(3)v^+=0$ transitions which have the same lower state $4f$, $N^+=2$, $N''=3$, $v^+=0$ (see Table I). The residual (observed−calculated) values of -0.272 and -0.252 cm^{-1}, respectively, agree to within 0.02 cm^{-1} indicating that the upper state levels are calculated correctly to within that amount while the $4f$ level is predicted 0.26 cm^{-1} too low by the *ab initio* theory.

Jungen, Dabrowski, Herzberg, and Vervloet[10] stated that the partial breakdown of the *ab initio* model for $4f$ is a result of the incomplete convergence of the perturbation expansion used to describe the electron−core interaction. The quality of the *ab initio* quantum defect curves is limited by the accuracy of this expansion. Errors in the quantum defect curves are expected to be greater for large R, since various polarizability tensor components become so large that perturbation theory does not describe the system accurately, and the higher-order terms in the expansion which are not included in the model are more significant at large R. It, therefore, follows that the errors in the *ab initio* approach are not due to the final stage of the calculation; that is, the errors are introduced prior to the rovibrational multichannel quantum defect treatment. Consequently, if one could obtain improved quantum defect functions over the range for which the required rovibrational wavefunctions of H_2^+ are significant, one would obtain more accurate energy predictions. We have used the averages of the observed singlet and triplet lines to obtain improved quantum defect functions. The fits were made to $4f$ energy levels, each of which was estimated by subtracting the $5g-4f$ experimental observation from the appropriate calculated *ab initio* $5g$ energy; this procedure is equivalent to fitting to the observed transitions. Most of the assigned levels included in the fit were calculated from the strong R branch transitions, but where Q and/or P branch transitions were available we have to take the appropriate average. Transitions for which only one line was observed were not included in the fit. The $4f$ levels associated with the observed lines $R_3(6)v^+=0$ and $R_3(6)v^+=2$ show abnormally large deviations and are thus apparently perturbed.

We denote the body-fixed quantum defect matrix elements as $\eta_{l,l'}^{(S,\Lambda,\Omega)}(\varepsilon,R)$ where S,Λ,Ω are the total spin, total orbital angular momentum component and total orbital plus spin angular momentum component, respectively. ε is the electron energy while R is the internuclear distance. l and l' are the orbital angular momentum quantum numbers of coupled channels (or Rydberg series). We consider only $l=l'$ in this work.

The *ab initio* quantum defect curves derived from the multipole polarization model[9] correspond to the average of $S=0$ and 1, which we shall call $\bar{S}$, and $\Omega=\Lambda$. They are used as a starting point and are represented as a second-order polynomial defined for a set of R values spanning the range 2.0 a.u.$\leqslant R\leqslant$3.2 a.u.

$$\eta_{ll}^{(\bar{S},\Lambda,\Omega=\Lambda)}(\varepsilon,R)=\eta_{ll}^{(\bar{S},\Lambda,\Omega=\Lambda)}(\varepsilon=0,R)+\frac{\delta\eta_{ll}^{(\bar{S},\Lambda,\Omega=\Lambda)}(R)}{\delta\varepsilon}\varepsilon+\frac{1}{2}\frac{\delta^2\eta_{ll}^{(\bar{S},\Lambda,\Omega=\Lambda)}(R)}{\delta\varepsilon^2}\varepsilon^2. \quad (4)$$

Since the present experimental data for the $4f$ state pertains only to one electron energy, $\varepsilon=-1/16$, it was decided to fit $\eta_{33}^{(\bar{S},\Lambda,\Omega=\Lambda)}(\varepsilon=0,R)$ over a limited range $R_{\rm lo}\leqslant R\leqslant R_{\rm hi}$, while retaining the *ab initio* values of $\delta\eta/\delta\varepsilon$ and $\delta^2\eta/\delta\varepsilon^2$. Due to the inherent smoothness of the quantum defect curves, it was decided that a parabola could serve as an adequate representation of the true curve over the relatively short range of internuclear separation required. The constants in this procedure are determined using parabolas of the form

$$\eta_{ll}^{(\bar{S}\Lambda\Omega)}(\varepsilon=0,R)=a_{ll}^{(\bar{S}\Lambda\Omega)}+b_{ll}^{(\bar{S}\Lambda\Omega)}x+c_{ll}^{(\bar{S}\Lambda\Omega)}x^2, \quad (5)$$

where x is taken to be $R-(R_{\rm lo}+R_{\rm hi})/2$; the x origin of the parabolas in this fit is, therefore, 2.6 Bohr.

To begin the fitting procedure, a simple second-order polynomial fit is obtained, in which the points to be fitted are the *ab initio* quantum defect function values against certain values of R; this is carried out between the lower and upper limits $R_{\rm lo}$ and $R_{\rm hi}$. The constant (a), linear (b), and quadratic (c) terms obtained are used to generate the initial quantum defect functions prior to the fit. For an f state, there are four Λ states: Σ, Π, Δ, and Φ. Each of these requires a quantum defect curve, and there is thus a total of twelve parameters. The initial quantum defect functions consist of three sections: The low $R(R<R_{\rm lo})$ region, in which the *ab initio* calculated points remain; the fitting region ($R_{\rm lo}\leqslant R\leqslant R_{\rm hi}$), in which the points are those generated by a parabola with constants defined as above; and the high $R(R>R_{\rm hi})$ region, in which the *ab initio* calculated points are again retained. These individual points are connected by cubic splines to give smooth quantum defect curves against R. In the fitting procedure, any or all of the twelve polynomial coefficients can be varied.

The use of a mixture of *ab initio* and fitted points for the quantum defect functions may seem strange; but the approach is justifiable for three reasons: Firstly, in the low R region, the *ab initio* quantum defect curves are expected to be accurate, so that there is little need for improvement; secondly, a parabola is not capable of describing the quantum defect functions well over a large range of R; and finally, one can only obtain a sensible fit over the range of R where the

TABLE II. Parameters obtained from MQDT least-squares fitting procedure for $4f$ Rydberg state of H_2 (see Sec. IV for definitions).

	Ab initio	Fitted
$a^{(\bar{S},\Sigma)}$	2.7316×10^{-2}	$2.6962(36)\times10^{-2}$
$b^{(\bar{S},\Sigma)}$	2.4802×10^{-2}	$2.4405(276)\times10^{-2}$
$c^{(\bar{S},\Sigma)}$	8.2389×10^{-3}	$0.8055(618)\times10^{-2}$
$a^{(\bar{S},\Pi)}$	2.1996×10^{-2}	$2.1703(42)\times10^{-2}$
$b^{(\bar{S},\Pi)}$	1.9740×10^{-2}	$1.9763(199)\times10^{-2}$
$c^{(\bar{S},\Pi)}$	6.4486×10^{-3}	$0.7393(471)\times10^{-2}$
$a^{(\bar{S},\Delta)}$	7.1629×10^{-3}	$0.7362(43)\times10^{-2}$
$b^{(\bar{S},\Delta)}$	6.7303×10^{-3}	$0.7579(176)\times10^{-2}$
$c^{(\bar{S},\Delta)}$	2.6311×10^{-3}	$0.3674(457)\times10^{-2}$
$a^{(\bar{S},\Phi)}$	-1.4453×10^{-2}	$-1.4579(41)\times10^{-2}$
$b^{(\bar{S},\Phi)}$	-9.7462×10^{-3}	$-1.0035(139)\times10^{-2}$
$c^{(\bar{S},\Phi)}$	-6.5209×10^{-4}	$-0.0897(405)\times10^{-2}$
$a^{(S=1,\Sigma)}-a^{(S=0,\Sigma)}$		$1.06(186)\times10^{-5}$
$a^{(S=1,\Pi)}-a^{(S=0,\Pi)}$		$4.47(288)\times10^{-5}$
$a^{(S=1,\Delta)}-a^{(S=0,\Delta)}$		$2.49(163)\times10^{-5}$
$a^{(S=1,\Phi)}-a^{(S=0,\Phi)}$		$1.76(118)\times10^{-5}$

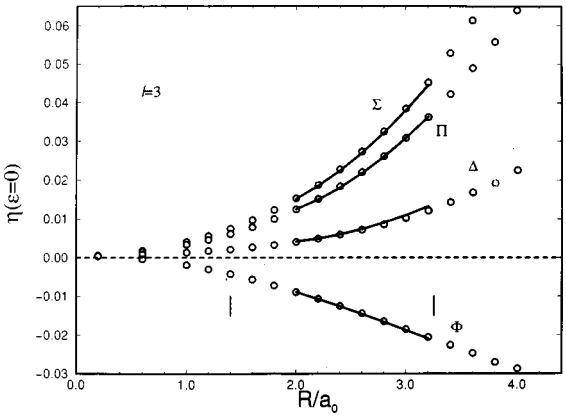

FIG. 2. *Ab initio* (circles) and fitted (full line) quantum defect functions for the Λ components of the $4f$ Rydberg state. The vertical bars indicate the classical inner and outer turning points for the vibrational motion in the $v^+=3$ state.

core rovibrational wave function in question has a significant amplitude. This latter point can be understood by considering the effect of the core rovibrational wave functions: They can be thought of in this context as statistical weight functions, since where there is little probability amplitude the calculated energies are not sensitive to the relatively small changes in the quantum defect functions which are necessary for the fit to be reasonable.

The implementation used in this work allowed fitting on a one-dimensional grid in R which has steps of 0.2 Bohr. The fitting region is defined as an odd number of points around a central point, and the most appropriate fitting region was found to be seven points at 2.6 Bohr, that is the range 2.0 to 3.2 Bohr. The vibrational channels $v^+=0-5$ were included in the calculations.

The overall quality of the fit is quite good. A comparison of the 50 singlet–triplet pairs of levels obtained from Table I and included in the fit with the appropriate *ab initio* predictions give a mean deviation of 0.33 cm^{-1}. Our fit (cf. Table I) yields a mean deviation (obs–calc) of 0.055 cm^{-1} for these same levels, i.e., not far from an order of magnitude less. This deviation corresponds to 1.6×10^{-5} on the quantum defect scale. The parameters determined in this fit are those of Table II and the corresponding fitted quantum defect curves are illustrated in Fig. 2, compared to the *ab initio* starting curves.

The MQDT program is able to account for electron spin and it has been used in a second stage of the fitting procedure to extract separate singlet and triplet quantum defects from the experimental data. The 20 para-H_2 (N^+ even) levels obtained from Table I which show no complicating hyperfine structure were used for this. Spin–orbit coupling is not included, so it is assumed that for given S and Λ the quantum defects do not depend on Ω. We, therefore, drop the superscript Ω in the following as well as the subscripts $l=l'=3$, and we determine the parameters $a^{(S=1,\Lambda)}-a^{(S=0,\Lambda)}$, $b^{(S=1,\Lambda)}-b^{(S=0,\Lambda)}$, $c^{(S=1,\Lambda)}-c^{(S=0,\Lambda)}$, respectively, while leaving the mean $(\bar{S})$ quantum defects constant, i.e., as determined in the first stage of the fitting. We found that we could not determine the triplet–singlet differences of the constants b and c and these were, therefore, constrained to zero. The last four parameters given in Table II correspond to this second fit. The singlet–triplet splittings of the para levels (cf. Table III) were reproduced moderately well with a mean standard deviation of 0.022 cm^{-1}, i.e., approximately three times less than the mean splittings of 0.061 cm^{-1} for the 20 para-H_2 splittings used in the fit. The fitted singlet–triplet separations $a^{(S=1,\Lambda)}-a^{(S=0,\Lambda)}$ are listed in Table II. Their uncertainties are rather large; in particular the value for $\Lambda=0$ is not well determined.

C. Satellite structure

A feature of the spectrum not previously observed[10,12] is the presence of weak satellites accompanying the singlet–triplet pairs. Figure 3 illustrates the fine structure of the $R_3(2)v^+=0$ transition. The observed satellite features are listed in Table IV together with the main singlet and triplet lines; in other instances, only one satellite is strong enough to be observable. The spacing between a satellite and a main line is almost constant and is $0.04\pm0.005\,cm^{-1}$ for most cases. In one case, $R_1(4)v^+=3$ (Fig. 4), where the splitting is large, an additional feature is seen between the singlet and triplet lines. Table IV clearly shows that the satellites appear only for transitions starting from odd rotational levels, that is, for ortho-hydrogen. The satellites were noted for almost all transitions with odd N^+ quantum numbers that were sufficiently intense, and none of the transitions originating from levels with even N^+ showed any sign of satellite structure. Therefore, it is natural to interpret this splitting as due to hyperfine interaction. The fact that the magnitude of the splitting is comparable to the hyperfine splitting in the ground state[24,25] of ortho-H_2^+ also points in this direction.

A qualitative understanding of the satellite structure can be obtained as follows. There are primarily two types of splitting to consider, namely the hyperfine structure of the isolated H_2^+ ion and the singlet–triplet splitting of the molecule which is due to the interaction of the Rydberg electron with the core. Since both the singlet–triplet splitting and the

TABLE III. Observed and calculated $4f$ singlet–triplet splittings (cm^{-1}). Observed values from *R* branch transitions unless indicated. Calculated values for para-H_2 lines only (see text).

v^+	N^+	N	Obs	Calc	(Obs–Calc)
0	0	3	0.072	0.075	−0.003
0	1	2	0.048		
0	1	3	0.044		
0	1	4	0.056		
0	2	1	0.067	0.081	−0.014
0	2	2	0.065	0.084	−0.019
0	2	3	0.049	0.055	−0.006
0	2	4	0.062	0.067	−0.005
0	2	5	0.072	0.079	−0.007
0	3	0	0.060		
0	3	1	0.047		
0	3	2	0.054		
0	3	3	0.042		
0	3	4	0.075		
0	3	5	0.047[a]		
0	3	6	0.089		
0	4	3	0.064	0.058	0.006
0	4	6	0.053	0.074	−0.021
0	5	4	0.059		
0	5	5	0.046		
0	5	8	0.056		
1	0	3	0.071	0.066	0.005
1	1	2	0.034		
1	1	3	0.048		
1	1	4	0.061		
1	2	1	0.048	0.070	−0.022
1	2	2	0.063	0.072	−0.009
1	2	3	0.056	0.047	0.009
1	2	4	0.070	0.057	0.013
1	2	5	0.109	0.069	0.040
1	3	0	0.063		
1	3	2	0.055		
1	3	3	0.042		
1	3	5	0.051		
1	3	6	0.069		
2	0	3	0.110	0.075	0.035
2	1	2	0.088		
2	1	3	0.056		
2	1	4	0.061		
2	2	1	0.029	0.078	−0.049
2	2	3	0.049	0.051	−0.002
2	2	5	0.076	0.056	0.020
2	3	3	0.039		
2	3	5	0.055		
2	3	6	0.039		
2	4	7	0.038	0.077	−0.039
3	1	2	0.072		
3	1	3	0.048		
3	1	4	0.101		
3	2	5	0.098	0.078	0.020
3	3	3	0.030		
3	3	6	0.086		

[a]Observed singlet–triplet splitting of the *Q* branch line.

hyperfine interaction (in the case of ortho-H_2) are small relative to the rotational structure of the ion core, Hund's case (d) prevails throughout. This means that the core rotational quantum number N^+ is very nearly defined, and the singlet and triplet manifolds remain separate with the total electron spin *S* well-defined as long as the hyperfine splitting is small relative to the singlet–triplet splitting. On the other hand, if the ion hyperfine structure dominates, the total core spin G^+

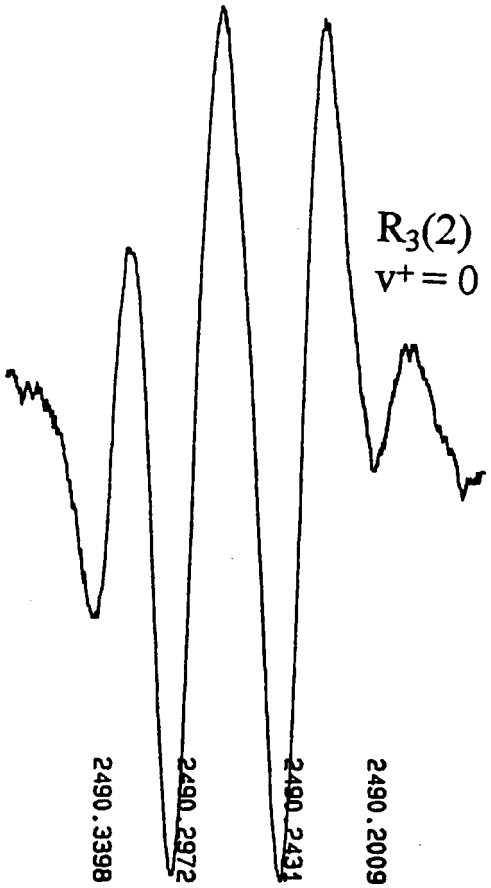

FIG. 3. $R_3(2)v^+=0$ transition of H_2 showing satellite structure.

(where $G^+=I+S^+$) will be very nearly defined and replaces *S*. It turns out that the $5g$ upper state falls into the latter category, while for the $4f$ state the two interactions are comparable and give rise to the observed multiplet structure.

This can be seen from the following: The singlet–triplet splitting which results from an electron–core interaction decreases rapidly with increasing *l* and is proportional to n^{-3}. The core hyperfine structure is of the order of 0.04 cm^{-1} (Jefferts[25]) for ortho-H_2^+ ($I=1$). For para-H_2^+ ($I=0$) the spin-rotation splitting is almost two orders of magnitude smaller. For ortho-hydrogen, we estimate from the known singlet–triplet splittings that for $l=1$ (p series) the uncoupling of the Rydberg electron spin from the core spin will take place near $n\sim100$ whereas for $l=4$ it is already complete at $n=5$.

For ortho-H_2, $G^+=I+S^+$ takes the values 1/2 and 3/2, the levels being separated by $\sim$0.04 cm^{-1}. In the $4f$ state the exchange interaction is off-diagonal and increases the total splitting from the ion core value of 0.04 cm^{-1} to about 0.08 cm^{-1}. In the main lines of the $5g-4f$ transition corresponding to $\Delta G^+=0$, the difference of the lower and upper state splittings is observed, i.e., $0.08-0.04=0.04\,cm^{-1}$ in agreement with the observed mean value of $0.05\pm0.01\,cm^{-1}$—see Table IV.

The satellite transitions $\Delta G^+=\pm1$ are separated by the sum of the upper and lower state splittings, and the distance of each satellite from the nearest line corresponds to the hyperfine splitting of the $5g$ upper state (0.04 cm^{-1}). It is clear

TABLE IV. Observed transitions (cm^{-1} units) with hyperfine structure. These are all due to ortho-hydrogen.

	Triplet		Singlet		
Transition	Satellite line	Main line	Main line	Satellite line	Central line
$v^+=1\ R_1(3)$			2459.444	2459.400	
$v^+=0\ R_1(3)$	2459.626	2459.582			
$v^+=2\ R_1(3)$			2459.949	2459.906	
$v^+=3\ R_1(3)$	2461.526	2461.463	2461.415	2461.379	
$v^+=0\ Q_3(4)$			2461.596	2461.548	
$v^+=0\ R_3(4)$	2463.562	2463.531	2463.456	2463.418	
$v^+=1\ R_3(5)$	2468.841	2468.803	2468.752	2468.716	
$v^+=0\ Q_3(5)$			2469.461	2469.425	
$v^+=0\ Q_3(3)$			2470.112	2470.086	
$v^+=2\ R_3(5)$			2470.345	2470.299	
$v^+=1\ Q_3(5)$	2470.834	2470.787	2470.734	2470.700	
$v^+=0\ R_3(3)$			2473.781	2473.734	
$v^+=0\ R_1(4)$	2489.395	2489.362	2489.306	2489.259	
$v^+=0\ R_3(2)$	2490.340	2490.297	2490.243	2490.201	
$v^+=1\ R_1(4)$	2494.322	2494.284	2494.223	2494.183	
$v^+=1\ R_3(2)$			2494.594	2494.546	
$v^+=0\ R_5(8)$	2495.218	2495.189	2495.133	2495.092	
$v^+=1\ R_3(6)$			2498.287	2498.244	
$v^+=0\ Q_1(4)$	2498.531	2498.483			
$v^+=0\ R_1(2)$	2498.720	2498.678	2498.630	2498.592	
$v^+=0\ Q_3(1)$			2501.057	2501.004	
$v^+=1\ R_1(2)$			2504.753	2504.701	
$v^+=3\ R_1(4)$	2508.421	2508.387	2508.286	2508.243	2508.325
$v^+=3\ R_3(6)$			2512.842	2512.798	
$v^+=1\ R_3(0)$	2519.842	2519.796	2519.733	2519.689	
$v^+=3\ R_1(2)$			2521.271	2521.227	

that the satellite lines are forbidden in both extremes.

In order to ascertain that this qualitative discussion is correct, we have carried out a full nuclear spin–electron spin–electronic–rotational MQDT calculation for one of the most prominent spectral lines, $R_3(2)v^+=0$, shown in Fig. 3. The details of this new development will be described in a forthcoming publication.[26] The main extension concerns the rotational frame transformation which now includes not only electron spin but also nuclear spin.

Briefly, the frame transformation used previously[27] connecting Hund's case (b) to Hund's case (d) has matrix elements of the form $\langle N^+|\Lambda\rangle^{(NMp,q^+,l)}$. The quantum numbers not previously specified are $M=$magnetic space quantum number, p for total parity, q^+ for core parity index ($q^+=1$ for Σ^- cores, zero otherwise). At present the frame transformation takes the form

$$\langle N^+G^+F^+j|S\Lambda\Omega J\rangle^{(FM_Fp;\Lambda^+S^+;i_1i_2I;q^+t^+;ls)}, \tag{6}$$

where the new quantum numbers are F^+, the core total angular momentum, G^+, the total core spin (electron plus nuclei) angular momentum, j is the total Rydberg electron angular momentum (orbital plus spin). F is the total molecular angular momentum (replacing N). i_1, i_2, and I are the nuclear spin quantum numbers and the total nuclear spin quantum number, respectively. t^+ gives the behavior of the electronic core wave function under the permutation of the two nuclei and $s=1/2$ is the spin of the Rydberg electron. The analytical expressions will be given later.[26]

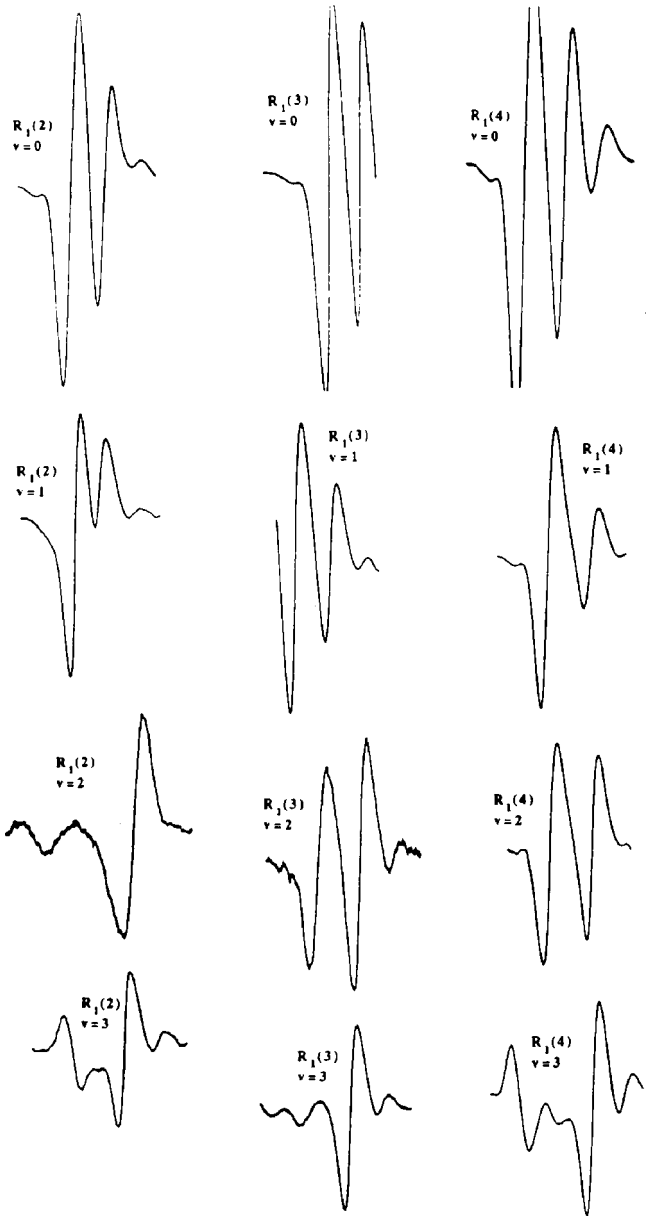

FIG. 4. Line shapes of $R_1(2)$, $R_1(3)$, and $R_1(4)$ transitions for sequence $v^+=0,1,2,3$ illustrating trend towards stimulated emission of triplet lines at higher v^+.

In the multichannel treatment, every hyperfine level of the ion becomes a separate ionization threshold. We have used the theoretical hyperfine levels calculated with the coupling constants of Babb and Dalgarno.[28] Correspondingly, the number of channels to be included increases substantially. For example, for the $5g$ $N=3$, $N^+=3$ state where we include only $v^+=0$, we have for $F=5$, $p=1$ a total of 53 channels in the calculation. Similarly for $4f$, $N=2$, $N^+=3$, including three vibrational channels ($v^+=0-2$) there are a total of 123 channels for $F=4$, $p=0$. The calculations were carried out with exactly the same quantum defects determined from the para-H_2 levels.

The upper level of the $R_3(2)$ line is at 120 374 cm^{-1}. The full calculation has 12 hyperfine components with F varying from one to five. The lower level of the $R_3(2)$ line is at 117 883 cm^{-1} and also has 12 components with F ranging

TABLE V. Theoretical hyperfine structure in the $v^+=0$, $N^+=3$, $5g$ and $4f$ states (cm^{-1} units).

$5g\ v^+=0,\ N^+=3$ Energy	$F(N=3)$
120 373.719 915	5
.719 915	4
.719 425	2
.719 425	1
.718 907	2
.718 902	3
.718 893	3
.718 848	4
.673 303	2
.673 302	3
.673 028	4
.673 027	3
$4f\ v^+=0,\ N^+=3$ Energy	$F(N=2)$
117 883.465 201	3
.464 171	2
.464 143	1
.414 857	4
.413 703	3
.413 470	0
.413 385	1
.413 365	2
.377 644	1
.377 454	2
.377 282	3
.367 832	2

from zero to four. These are listed in Table V. A representation of the calculated upper and lower levels of the $R_3(2)$ line is shown in Fig. 5. It can be seen that the levels occur in two groups for the $5g$ level, and four groups for the $4f$ level.

The preceding qualitative discussion of the energy level structure of the $5g$ and $4f$ levels can now be refined. We see [Fig. 5(a)] that in the $5g$ state the hyperfine structure indeed prevails such that $G^+=1/2$ and 3/2 is approximately a good quantum number and the characteristic ion splitting of 0.04 cm^{-1} is apparent. The statistical weight of the $G^+=3/2$ component (8 levels) is twice that of the $G^+=1/2$ component (4 levels), as expected (an additional factor of 2 arises from the spin of the $5g$ electron). The splitting of the sublevels F (not entirely resolved on the scale of the figure) is due to interaction of G^+ with the nonspherical molecular field.

Turning now to the $4f$ state [Fig. 5(b)] we see an intermediate situation, neither the core hyperfine structure nor the singlet–triplet splitting dominates. In the singlet–triplet terminology one would say that the lower three groups (9 levels) constitute the triplet state whereas the upper group (3 levels) constitutes the singlet state. However, 5 triplet states are about to ''migrate'' up toward the singlet group. In other words, a pattern similar to Fig. 5(a) with 8 upper and 4 lower levels is about to form. Starting from the pattern of Fig. 5(a) [and reducing each F value of Fig. 5(a) by 1], we see that the off-diagonal singlet–triplet interaction must leave the single $F=0$ and $F=4$ levels undisturbed. The interactions between the remaining $F=1$, 2, 3 levels involve for each F a pair of levels in the upper manifold of Fig. 5(a). Degenerate perturbation theory then tells us that one member of each pair is left undisturbed while the other member is shifted upwards. The pattern of Fig. 5(b) is hence obtained.

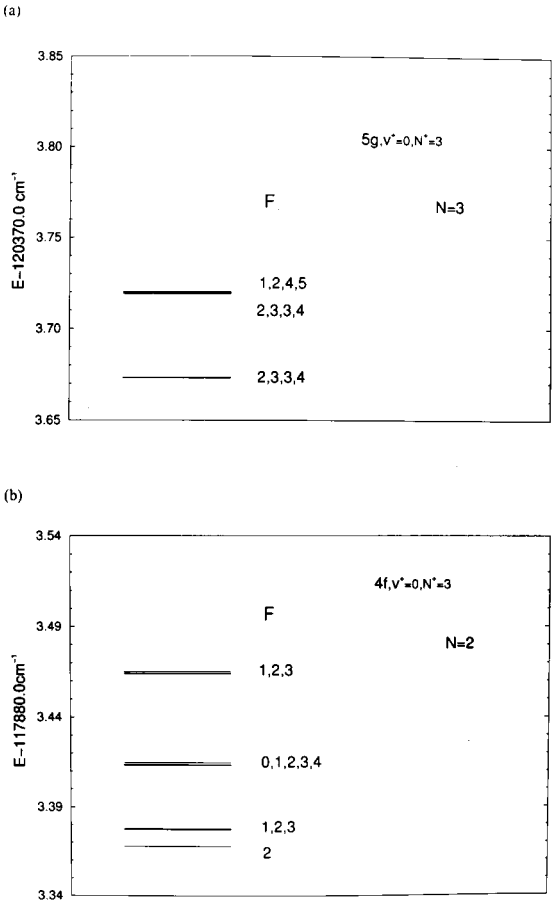

FIG. 5. Calculated hyperfine level structure of (a) the $5g$, $v^+=0$, $N^+=3$, $N=3$ and (b) the $4f v^+=0$, $N^+=3$, $N=2$ levels of H_2.

The intercombination between these sets of levels yields 83 allowed transitions, which come in 4 groups as shown in Fig. 6 where the spectrum has been convoluted with a 0.025 cm^{-1} experimental linewidth broadly giving the observed experimental contour, Fig. 3. Fig. 6 indicates for comparison the positions and intensities of the observed lines. It can be seen that the positions are very well reproduced whilst the

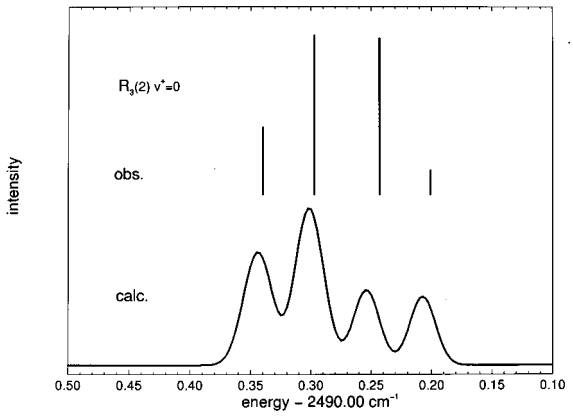

FIG. 6. Calculated $R_3(2)v^+=0$ transition including hyperfine splittings. The full spectrum consists of 83 transitions. These have been convoluted with an assumed experimental width of 0.025 cm^{-1}. The positions of the observed components are indicated by vertical bars whose length correspond roughly to the observed intensities.

agreement is only fair as far as the intensities are concerned: Further calculations for other ortho-H_2 lines should enable the analysis of the different observed patterns (see Table IV).

V. NONTHERMAL POPULATIONS AND STIMULATED EMISSION LINES

For each $5g-4f$ Rydberg transition, the triplet line is expected to be more intense due to the electron spin statistics of 3:1 and to occur at a slightly higher frequency than the corresponding singlet; this is the case for many of the assigned lines. However, we have often observed that the relative intensities of the two lines were very different; there were cases where the triplet line was weaker than the singlet or only one line was present in the spectrum. Moreover, the phase of the first derivative line shape was reversed in two of the triplet transitions. The observed intensity ratios between the singlet and triplet lines of a given transition were found to be different from those observed in the FTIR study,[10] especially for relatively highly vibrationally excited levels.

There is an approximate systematic trend for the variation of the relative intensities as we follow the series of transitions with the same rotational quantum numbers but different vibrational states. For $v^+=0$ transitions, the triplet lines were always more intense than the singlet lines. For $v^+=1$ and $v^+=2$ transitions, the range of triplet-to-singlet intensity ratios varied widely, or only one line was observed. In the $v^+=3$ transitions, the triplet was weaker than the singlet, and two of the triplet lines had inverted line shapes. This progression with v^+ is illustrated for the transitions $R_1(2)$, $R_1(3)$, and $R_1(4)$ in Fig. 4.

These anomalies are best explained as due to a nonthermal distribution of population in triplet $5g$ versus $4f$ states. The reversal of the phase of the first derivative line shape demonstrates stimulated emission and thus the population inversion between the $5g$ and $4f$ levels for high vibrational states. This phase inversion has also been observed in the diode laser spectra,[12] although the inverted line was not assigned. Such population inversion leading to laser action has been reported by McKnight and Barr[29] and assigned by Dabrowski and Herzberg [30] for the $a\,^3\Pi-c\,^3\Pi_u$ transitions. Dabrowski and Herzberg explain the population inversion as due to predissociation of the $^3\Pi_u$ state resulting from a mixing with the dissociative $^3\Sigma_u^+$ curve. A similar explanation may be possible for our observation of the population anomaly only in certain triplet states. Such a population inversion will be more easily sustainable in higher vibrational levels.

VI. CONCLUSION

The observation of hitherto unobserved Q branch $5g-4f$ transitions has helped to confirm previous R-branch assignments, and the number of the $5g-4f$ assignments has been substantially increased compared to previous studies. The determination of effective multichannel quantum defect functions by a least-squares fitting procedure has been shown to improve considerably the accuracy of the calculated transition frequencies for the assigned lines. In a second stage, this is extended to include the fitting of separate singlet and triplet quantum defect parameters.

The high sensitivity and resolution of the difference frequency technique has revealed previously unobserved satellite features which are interpreted as being predominantly due to the Fermi contact hyperfine interaction. The appearance of this structure along with the ''singlet'' and ''triplet'' lines indicates that the $4f$ state of ortho-hydrogen is in an intermediate situation where neither the total electron spin S nor the total core spin G^+ (electron plus nuclear) is well defined. The $5g$ state on the other hand corresponds to well defined G^+. Thus although the $5g-4f$ transitions are labeled as singlets and triplets, this description is only an approximation for the odd N^+ transitions. A sample MQDT calculation, including hyperfine interaction, confirms the analysis of the observed satellite structure due to electronic and nuclear spin coupling within the $v^+=0$, $N^+=3$, $N'=3 \leftarrow v^+=0$, $N^+=3$, $N''=2$ transition.

The capability of laser spectroscopy to observe the Rydberg transitions in absorption has revealed a population anomaly leading to stimulated emission for some triplet transitions corresponding to relatively high vibrational levels. This may be attributable to predissociation of the triplet levels due to interaction with the $4p$ state.

[1] Ch. Jungen and E. Miescher, Can. J. Phys. **47**, 1769 (1969).
[2] A. D. Buckingham, Discuss. Faraday Soc. **40**, 232 (1965).
[3] F. J. Basterrechea, P. B. Davies, D. M. Smith, and R. J. Stickland, Mol. Phys. **81**, 1435 (1994).
[4] P. A. Martin, R. J. Stickland, C. S. B. Martin, and P. B. Davies, Can. J. Phys. **72**, 979 (1994), and references therein.
[5] K. P. Huber, Ch. Jungen, K. Yoshino, K. Ito, and G. Stark, J. Chem. Phys. **100**, 7957 (1994).
[6] M. R. Dobber, W. J. Buma, and C. A. de Lange, J. Chem. Phys. **101**, 9303 (1994).
[7] M. S. Child and W. C. Glab, J. Chem. Phys. **112**, 3754 (2000).
[8] G. Herzberg and Ch. Jungen, J. Chem. Phys. **77**, 5876 (1982).
[9] Ch. Jungen, I. Dabrowski, G. Herzberg, and D. J. W. Kendall, J. Chem. Phys. **91**, 3926 (1989).
[10] Ch. Jungen, I. Dabrowski, G. Herzberg, and M. Vervloet, J. Chem. Phys. **93**, 2289 (1990).
[11] P. B. Davies, M. A. Guest, and R. J. Stickland, J. Chem. Phys. **93**, 5408 (1990).
[12] P. B. Davies, M. A. Guest, and R. J. Stickland, J. Chem. Phys. **93**, 5417 (1990).
[13] W. G. Sturrus, E. A. Hessels, P. W. Arcuni, and S. R. Lundeen, Phys. Rev. A **44**, 3032 (1991), and references therein.
[14] W. G. Sturrus, E. A. Hessels, P. W. Arcuni, and S. R. Lundeen, Phys. Rev. A **38**, 135 (1998).
[15] C. H. Greene and Ch. Jungen, Adv. At. Mol. Phys. **21**, 51 (1985).
[16] M. G. Bawendi, B. D. Rehfuss, and T. Oka, J. Chem. Phys. **93**, 6200 (1990).
[17] G. Guelachvili and K. N. Rao, *Handbook of Infrared Standards* (Academic, New York, 1986).
[18] R. L. Day and R. J. Anderson, J. Chem. Phys. **71**, 3683 (1979).
[19] H. A. Bethe and E. E. Salpeter, *Quantum Mechanics of One and Two Electron Atoms* (Springer-Verlag, Berlin, 1957).
[20] P. M. Dehmer and W. A. Chupka, J. Phys. Chem. **99**, 1686 (1995).
[21] J. D. Shao and C. Y. Ng, J. Chem. Phys. **84**, 4317 (1986).
[22] A. J. Yencha, in *Electron Spectroscopy, Theory, Techniques, and Applications, Vol. 5, Penning Ionization and Related Processes*, edited by C. R. Bundle and A. D. Baker (Academic, London, 1984).
[23] S. C. Ross and Ch. Jungen, Phys. Rev. A **49**, 4364 (1994).
[24] Z. W. Fu, E. A. Hessels, and S. R. Lundeen, Phys. Rev. A **46**, R5313 (1992).
[25] K. B. Jefferts, Phys. Rev. Lett. **23**, 1476 (1969).

[26] A. Wüest and Ch. Jungen (in preparation).
[27] Ch. Jungen and G. Raseev, Phys. Rev. A **57**, 2407 (1998).
[28] J. F. Babb and A. Dalgarno, Phys. Rev. A **46**, R5317 (1992).
[29] W. B. McKnight and T. A. Barr, Appl. Opt. **21**, 357 (1982).
[30] I. Dabrowski and G. Herzberg, Acta Phys. Hung. **55**, 219 (1984).
[31] See EPAPS Document No. E-JCPSA6-113-014046 for complete line listing of all observed transitions: This document may be retrieved via the EPAPS homepage (http://www.aip.org/pubservs/epaps.html) or from ftp.aip.org in the directory /epaps/. See the EPAPS homepage for more information.